

Perturbation Effect of Fiducial Marker on 3D Dose Distribution in External Surrogates Radiotherapy

Ahmad Esmaili Torshabi^{1*}, Masoud Taghipour¹

1. Faculty of Sciences and Modern Technologies, Graduate University of Advanced Technology, Kerman, Iran

ARTICLE INFO	ABSTRACT
Article type: Original Paper	Introduction: Tumor motion is a challenging issue in radiotherapy, which complicates the process of tumor delineation, localization, and dose delivery. External surrogate radiotherapy is one of the available strategies that provides motion dataset for a consistent prediction model to track tumor motion using internal-external markers. Regarding this, the present study was conducted to investigate the effect of implanted fiducial on 3D uniform dose distribution.
Article history: Received: Nov 08, 2019 Accepted: Jan 12, 2020	Material and Methods: For the purpose of the study, a Monte Carlo code was utilized to simulate clip with different dimensions and material structures against four therapeutic beams. Moreover, a combinational clip made of golden and covered by polymethyl methacrylate (PMMA) was proposed to be used with lower dose perturbation. Finally, it was proposed to implant a clip outside tumor volume at specific distances from tumor site to keep dose uniformity on tumor volume. To investigate this issue, the correlation coefficient parameter was calculated as the metric among the motion dataset of tumor and clip.
Keywords: Radiotherapy Fiducial Marker Radiation Dosage Monte Carlo method	Results: Based on the results, dose perturbation caused by implanted clip was remarkable at hadron therapy depending on its size and material, mainly at the downstream part of the clip. Conclusion: As the findings indicated, the golden marker covered with PMMA could remarkably reduce dose perturbation. The most important concern in this domain is the presence of a possible correlation between tumor motion and motion of the clip implanted outside the tumor volume. The results of the correlation coefficient revealed a close relationship between tumor motion and clip motion.

► Please cite this article as:

Esmaili Torshabi A, Taghipour M. Perturbation Effect of Fiducial Marker on 3D Dose Distribution in External Surrogates Radiotherapy. Iran J Med Phys 2021; 18: 96-105. 10.22038/ijmp.2020.44330.1677.

Introduction

External beam radiotherapy (EBRT) is a common cancer therapeutic modality that uses a machine to deliver a prescribed high dose to the tumor volume from outside the patient's body. The purpose of EBRT is to deliver a prescribed dose to planning target volume and simultaneously minimize the received dose in the nearby healthy tissues. The therapeutic beams damage cancer cells and shrink tumor volume after each treatment session. In order to reduce side effects, the tumor must be delineated accurately in the treatment planning process at the initial stage and then aligned carefully against the therapeutic beam during the dose delivery step. Therefore, a better targeting accuracy may yield better treatment quality. There are several strategies to enhance targeting accuracy in image-guided radiotherapy (IGRT) [1-4].

Target localization is problematic in the thoracic region of the patient body given the tumor motion induced by breathing. This movement may increase the possibility of dose delivery to the surrounding healthy tissue, thereby causing serious side effects. Moreover, this motion increases the target definition uncertainties and setup errors, resulting in the delivery of higher or lower doses to the tumor volume.

There are several strategies, including direct X-ray imaging and external surrogate radiotherapy, to enhance the targeting accuracy [1-4].

The effect of tumor motion errors can be compensated by means of such strategies as breath-holding [5,

6], respiratory motion gating [7-9], and real-time tumor tracking [10]. The two latter cases required real-time information regarding the motion of dynamic tumors. Such information can be achieved by the installment of some motion monitoring systems at the treatment room to track tumor motion. These systems are various in performance and range from continuous X-ray imaging systems (e.g., fluoroscopy) to external surrogate-based technique. The latter technique is implemented to minimize the imaging dose received by patients in comparison with the fluoroscopy-based treatment strategy. In the external surrogate radiotherapy, the tracing of tumor motion is accomplished on the basis of a correlation between the motion information of internal markers implanted inside the tumor volume and external surrogates [11-19]. Therefore, a consistent and reliable correlation model should be developed at the pre-treatment stage

*Corresponding Author: Tel: Telephone: +989386730223; Fax: +983433776617; E-mail: ahmad4958@gmail.com, a.esmaili@kgut.ac.ir

based on the motion dataset of external surrogates and internal markers, known as training dataset. It should be noted that the training dataset is gathered with the aid of an optical tracking system (for detecting external markers location) and stereoscopic X-ray imaging (for detecting internal marker location) in a synchronized mode.

A correlation model configured based on patient setup can facilitate the estimation of tumor location with an acceptable uncertainty error using the motion information provided by external surrogates [20-25]. Our recent works involved a comprehensive assessment of the performance of various correlation models to verify their pros and cons [26-28]. Tumor location is also detected alternately during the treatment using stereoscopic X-ray imaging for two purposes, namely testing the model performance accuracy and updating the model parameters.

In some patients, X-ray images have low radiographic contrast failing to specify the typical coordinate of the tumor volume. In order to solve this issue, some fiducial markers are implanted inside or near the tumor volume to properly visualize the entity. In this way, marker motion represents tumor motion and provides 3D tumor position information. Moreover, in some cases, a natural anatomical landmark with high-contrast property, such as the rib cage bony structure, is represented as an internal marker. In the clinical practice of IGRT, fiducial markers are implanted to verify tumor location at patient setup and during treatment for aligning the tumor against the therapeutic beam [29-32].

The main role of a fiducial marker is to provide good radiographic visibility in stereoscopic X-rays at the patient setup step. The provided dataset at the pre-treatment step, known as training dataset, is used to learn and construct a correlation model. However, the implantation of fiducial inside patient body may raise several concerns. This marker should not migrate throughout the treatment time and must be harmless and nontoxic to patient body. Moreover, from medical physicists' point of view, fiducial(s) should not perturb the 3D uniform dose, prescribed for the tumor volume per irradiation fraction [33].

Recent investigations have shown that fiducial markers can cause perturbation in the planned dose [34-44]. This perturbation results from the collision of the primary therapeutic beam with an internal marker and production of secondary particles, such as backscattered electrons. Moreover, the presence of an internal marker or clip along the therapeutic beam may affect the primary beam energy and result in dose uniformity. Therefore, the uniformity of the delivered dose is disturbed, while the amount of dose at the upstream and downstream of the marker are not the same. It should be noted that the amount of dose perturbation depends on location, material, geometry, and orientation against the therapeutic beam [35,36, 39].

The present study was targeted toward investigating comprehensively the effect of implanted clip on dose perturbation in conventional radiotherapy with photon and electron beams and also in hadron therapy with proton and carbon ion beams. The significance of dose uniformity, as the main objective, in radiotherapy highlights the importance of considering the role of implanted clip in dose uniformity disturbance. The researchers of the current study also proposed the use of a combinational clip made by golden material covered by PMMA (polymethyl-methacrylate) that may remarkably reduce dose perturbation.

Moreover, the present study involved the investigation of several optimum locations for internal clip outside the tumor volume that has not been assessed in previous research. To this end, a Monte Carlo simulation study was performed to quantitatively assess the role of internal clip in 3D dose distribution taking into account different therapeutic beams. Moreover, a strategy was proposed to find an optimum location for the internal clip outside the tumor volume using 4D XCAT anthropomorphic phantom developed by Dr. WP Segars [45]. This phantom can account for the respiratory motion of different organs and their anatomical details as the function of time. This phantom provides accessibility to each internal dynamic organ for any desired investigation, such as the definition of tumor with any size at any site with regard to clip location. Implementation of the same assessment in real condition with a real patient is impossible.

In the strategy proposed in this study, dose distribution in tumor volume will be kept uniform, and the most concern is about the presence of an acceptable correlation between tumor motion and clip motion implanted outside the tumor volume. In other words, the most important issue that must be investigated while using this strategy is to ensure whether the outside clip can still be a good representative of tumor motion. To this end, a typical internal clip was simulated at different distances from the lung tumors located at various sites using XCAT, and the correlation between tumor motion and clip motion was quantitatively assessed.

The results demonstrated that clip implantation resulted in a higher perturbation in hadron beams than in photon and electron beams. This is due to the physical properties of protons and heavy ions interactions with the matters of the clip, such as linear energy transfer (LET) and Bragg curves energy deposition. The use of a combinational golden marker covered with PMMA remarkably reduced dose perturbation. It should be noted that the use of a combinational clip, its mechanical resistance, and its contrast at stereoscopic X-ray images remained constant. Moreover, our results revealed that implanting a clip outside the tumor volume was

clinically possible and could be representative of dynamic tumors since there was a close correlation between tumor motion and clip motion up to a specific distance.

Materials and Methods

FLUKA code

The simulation of dose distribution in the tumor volume was accomplished using the Monte Carlo FLUKA code (version 2011) developed by CERN (European Organization for Nuclear Research) and INFN (Italian National Institute for Nuclear Physics). The FLUKA is a validated Monte Carlo simulation package for modeling particle transport and interactions with a matter. The FLUKA can be used for shield design, medical physics, dosimetry calculation, calorimetry, detector design, and radiotherapy. Moreover, it can simulate many types of particles (about 60 different particles) in matter with high-accuracy interaction and propagation. The FLUKA can also simulate very complex geometries through an improved version of the well-known combinatorial geometry package [46,47].

Simulation setup

A golden marker was simulated in a cylindrical shape at three small (0.4 mm in diameter), medium (0.8 mm in diameter), and large (1.2 mm in diameter) dimensions. The length of the simulated cylindrical clip was 3 mm. It was proposed to reduce the dimension of the golden clip and cover it with PMMA material known as the combinational clip. This may remarkably reduce a possible perturbation caused by the clip. This strategy was investigated in our simulation process, and the results were compared with one another. Figure 1 depicts a schematic presentation of the golden clip covered by PMMA material.

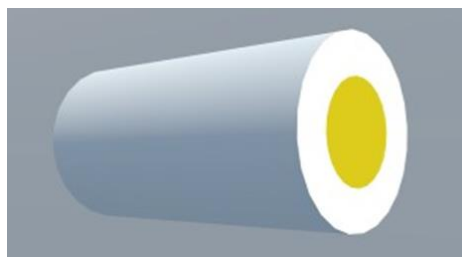


Figure 1. Combinational clip and golden marker (inner part) covered with PMMA (outer part)

A spherical tumor volume with a 1-cm diameter was modeled into a soft tissue cubic shape with a 10*10-cm dimension (Figure 2). The materials of the tumor and soft tissue were defined according to the International Commission on Radiological Protection (ICRP) standards [48]. The effect of different markers of different dimensions and materials on dose perturbation along the clinical therapeutic beams was investigated in our simulation process. The obtained results were compared with one another and with a condition while no marker was utilized as a reference. A schematic presentation of this simulation study is illustrated in Figure 2. The presence of the marker inside (left side) and outside (right side) the spherical tumor volume is depicted in Figure 2.

Four different therapeutic beams were simulated in this study. These beams included 6 MV-photon, 10-MeV electron, 100-MeV proton, and 200-MeV carbon. In our simulation setup, the marker was perpendicular to the beam central axis. The field size of simulated beams was the same as the lateral size of tumor volume for all beams. For proton and carbon ion beams, a 1-cm spread-out Bragg peak (SOBP) was defined to cover the longitudinal direction of the tumor in depth. To this end, the two types of ridge filters were simulated to give 1 cm SOBP as a longitudinal flat region. It should be noted that the location of the implanted clip was in the middle of the generated SOBP.

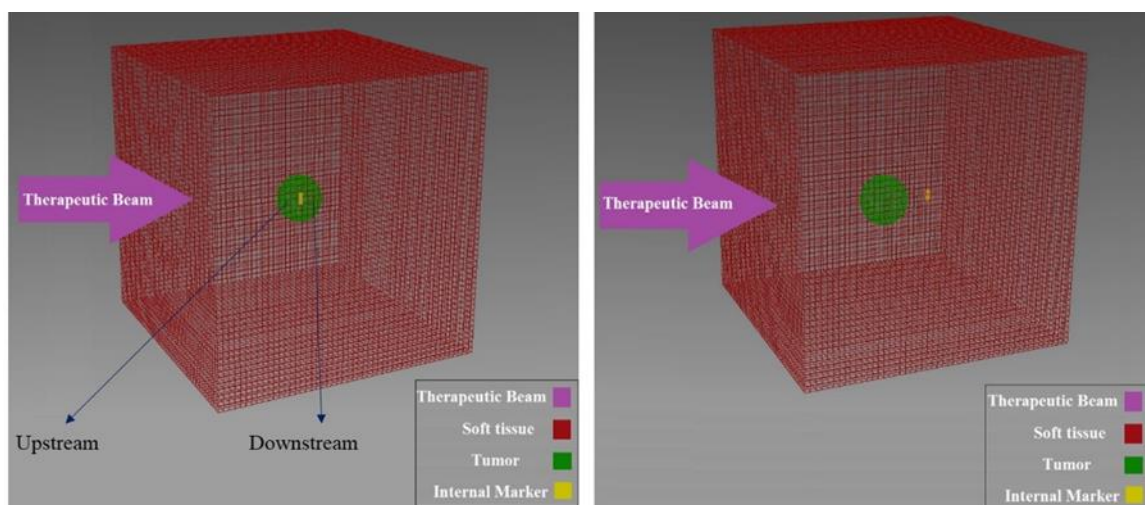


Figure 2. A schematic presentation of a typical clip (yellow) inside (left) and outside (right) the tumor volume (green) at normal soft tissue structure (red) along the therapeutic beam

In order to minimize the statistical uncertainty or standard deviation of simulation output and keep it within an acceptable range (i.e., <5%), 10×10^6 particles were taken into account at each simulation cycle. It should be noted that the simulation process was performed using a computer system with a CPU speed of 2.13 GHz and 4 gigabytes of RAM.

XCAT phantom and its properties

As mentioned above, in order to avoid dose perturbation, the internal clip was proposed to be implanted outside the tumor volume. This practice facilitated not only the achievement of the contrast required for tumor monitoring but also the maintenance of the uniformity parameter of dose distribution onto tumor volume. We also assessed the most challenging issue of this idea that is the possible correlation of outer clip motion with tumor motion.

To this end, a modeling study was accomplished by means of a 4D XCAT anthropomorphic phantom, (developed by Dr. Paul Segars at Duke University, USA). This validated phantom is commercially available for research activities, and the simulation results derived from this phantom can be helpful for clinical treatment [49-58]. This phantom has been developed to simulate the shapes, structures, and materials of complex organs in the human body. The 4D XCAT phantom also consists of the motion properties of dynamic organs, such as the respiratory system [45]. This property is highly applicable in our research field, especially in tumor tracking radiotherapy. It should be noted that the concept of XCAT phantom is based on the combination of pixelized and flexible phantoms that enables more accurate modeling of dynamic cases [59].

The XCAT phantom works using the Spline mathematical approach consisting of human anatomy and dynamic information of breathing and heartbeat.

The key point of this phantom is changing functional variables that control respiration and heartbeat. Therefore, the user is able to generate deformable 4D CT models according to the condition of a typical real patient organ motion that must be simulated. The main controllable options of this phantom are: 1) motion pattern option for beating heart only, respiration only, or combined mode, 2) maximum diaphragm motion in the superior-inferior direction, 3) maximum anterior-posterior expansion of the chest wall, and 4) anatomical characteristics, such as organ size. Figure 3 depicts some tomographic images of XCAT phantom with a lung tumor at two breathing phases.

In order to enhance the accuracy of our modeling process, the required parameters of XCAT phantom were defined according to the motion information of real patients. For instance, the first and third options were defined according to the breathing information of real patients treated with the Cyberknife Synchrony System [26]. Table 1 illustrates the use of the respiratory motion information of patients for pre-defined parameters in the anthropomorphic phantom to mimic the real respiratory pattern.

In the XCAT phantom, we defined four lung tumors in the left (Ltumor1 and Ltumor2) and right (Rtumor1 and Rtumor2) sides of the lung region as shown in Figure 4. Tumors were assumed to locate behind the second and third ribs (Figure 4).

For each tumor, a fiducial was taken into account located at various distances from the tumor for measuring the available correlation. It should be noted that the parameters of internal dynamic organs located at the thorax of this phantom could be varied and also each arbitrary clip or tumor could be simply defined at each coordinate of desired organs. Accordingly, this investigation could not be performed on a real patient.

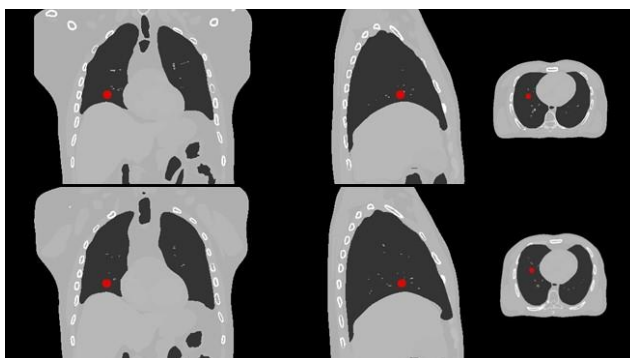


Figure 3. Tomography typical images taken from XCAT phantom with defined tumors (red spots)

Table 1. Tunable parameters of XCAT phantom to mimic real respiratory pattern

Breathing cycle number	Time of respiratory period (sec)	Maximum diaphragm motion (cm)	Maximum anterior-posterior expansion of chest wall (cm)
1	5	2	1.2
2	5	1.7	0.7
3	4	1.2	0.5
4	6	2.2	1.3
5	5.5	1.8	1
6	3.5	1	0.5

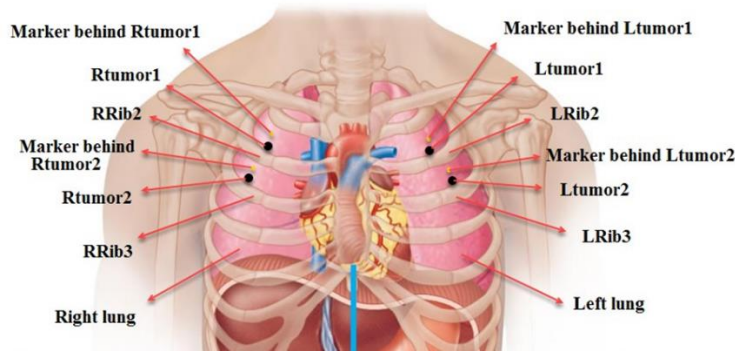


Figure 4. Schematic front view of lung region with four left and right tumors (dark spot) and implanted clips (yellow point) defined near the 2nd and 3rd ribs (Ltumor1: Left tumor behind rib #2, Ltumor2: Left tumor behind rib #3, Rtumor1: Right tumor behind rib #2, Ltumor2: Right tumor behind rib #3)

Table 2 shows the distances considered between the right/left tumor and implanted clip. To make a consistent correlation between tumor and clip motion dataset, the correlation coefficient parameter was utilized as the mathematical metric tool. The correlation coefficient is a proper criterion for determining the degree of correlation between two groups of variables, calculated as follows:

$$R_{MT} = \frac{\overline{M \times T} - \overline{M} \times \overline{T}}{\sqrt{S_M^2 \times S_T^2}}$$

$$\overline{M} = \frac{1}{n} \sum M_i, \quad \overline{T} = \frac{1}{n} \sum T_i, \quad \overline{M \times T} = \frac{1}{n} \sum M_i T_i$$

$$S_M^2 = \overline{M^2} - \overline{M}^2, \quad S_T^2 = \overline{T^2} - \overline{T}^2 \tag{1}$$

where “ R_{MT} ” is the correlation coefficient between clip and tumor, “ M ” is clip position information, and “ T ” is tumor position information.

Table 2. Distances between markers and defined right and left lung tumors

Marker number	Distance between marker and left lung tumor (mm)	Distance between marker and right lung tumor (mm)
1	2	6
2	8	12
3	14	18
4	20	24
5	26	30
6	32	36
7	38	42
8	44	48
9	50	54
10	56	60
11	62	66
12	68	72
13	74	78
14	80	84
15	86	90

Results

Tables 3 and 4 present the effect of dose perturbation by an implanted clip at the downstream and upstream parts of the clip position (beam propagation direction, shown in Figure 2), respectively. Dose variations were compared with the reference condition while no clip was utilized. As indicated in Table 3, the maximum dose perturbation occurred as a result of implanting a large golden marker along the carbon ion therapeutic beam. In contrast, the minimum value of dose perturbation was observed for the small golden marker using photon as the therapeutic beam. To perform this calculation, a specific volume with an optimal value of 15.84 mm³ was assumed around the implanted clip at both downstream and upstream sides of the clip, and the dose value was calculated in Gy. The use of the PMMA-golden combinational clip resulted in a remarkable decrease in dose perturbation, mainly for the carbon ion beam.

For better illustration, figures 5 and 6 graphically represent dose perturbation (increase or decrease) caused by the clip with regard to the reference condition. In these figures, dose values were normalized versus the reference condition where no marker was implanted. As seen, the maximum variation belongs to the downstream part of the large golden clip (Figure 5).

For instance, dose distribution variations for proton beam are shown in more detail in Table 5. As seen in this table, dose distribution is calculated at different locations of tumor volume in the depth direction range of 6.08-6.92 cm. In this table, the highlighted row represents dose value in a location where the clip exists. The maximum dose perturbation was close to the clip location at both upstream and downstream conditions.

Table 3. Dose perturbation caused by implanted clip at different conditions in comparison with reference (highlighted) at the downstream part of the clip

Beam type	No clip (Reference)	Small golden clip	Medium golden clip	Large golden clip	Combinational clip
Photon	0.0113	0.0112	0.0111	0.0108	0.0110
Electron	0.0685	0.0622	0.0502	0.0391	0.0614
Proton	0.5307	0.5162	0.4337	0.2319	0.5066
Carbon	2.9113	2.7907	1.7197	0.4924	2.6918

Table 4. Dose perturbation caused by implanted clip at different conditions in comparison with reference (highlighted) at the upstream part of the clip

Beam type	No clip (reference)	Small golden clip	Medium golden clip	Large golden clip	Combinational clip
Photon	0.0115	0.0118	0.0121	0.0125	0.0116
Electron	0.0698	0.0701	0.0710	0.0716	0.0704
Proton	0.5364	0.5345	0.5348	0.5352	0.5325
Carbon	2.8204	2.7911	2.8053	2.8005	2.7919

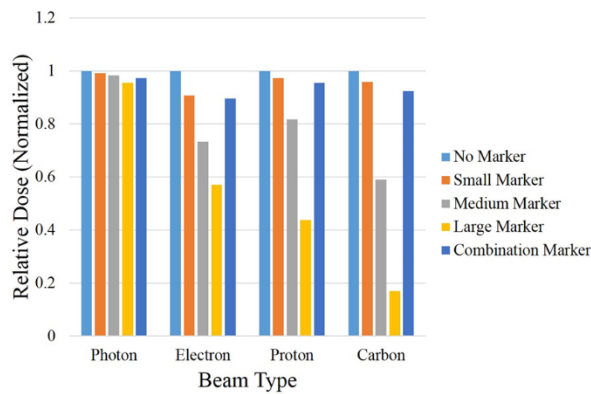


Figure 5. Relative dose variations in the downstream part of implanted marker against four therapeutic beams

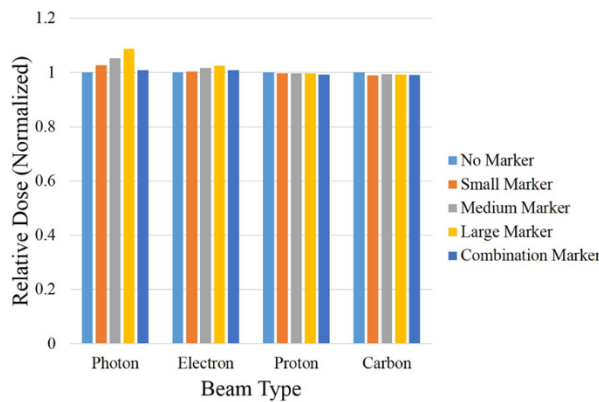


Figure 6. Relative dose variations in the upstream part of implanted marker against four therapeutic beams

Table 5. Detailed information of dose perturbation at different locations inside tumor volume at different depths

Depth in tumor	No clip (Reference)	Small golden clip	Medium golden clip	Large golden clip	Combinational clip
6.08 – 6.2	0.1450	0.1436	0.1464	0.1451	0.1446
6.2 – 6.32	0.1477	0.1473	0.1479	0.1475	0.1469
6.32 – 6.44	0.1490	0.1477	0.1497	0.1480	0.1471
6.44 – 6.46	0.0250	0.0247	0.0252		
6.46 – 6.48	0.0250	0.0246			
6.48 – 6.50	0.0499	0.1439	0.4766	0.2608	0.9448
6.50 – 6.52	0.0255	0.0254			
6.52 - 6.54	0.0255	0.0254	0.0251		
6.54 – 6.56	0.0255	0.0254	0.0251		
6.56 – 6.68	0.1498	0.1485	0.1399	0.0964	0.1487
6.68 – 6.8	0.1466	0.1414	0.1202	0.0605	0.1414
6.8 – 6.92	0.1443	0.1336	0.1029	0.0466	0.1334

As mentioned previously, in order to keep dose uniformity, a strategy was proposed to implant clip outside the tumor volume; however, the most concern was about a possible correlation between tumor and clip motions. This correlation was assessed quantitatively using the correlation coefficient parameter, and the results are reported in Figure 7. Four lung tumors were taken into account behind ribs #2 and #3, and correlation coefficient parameter was calculated at different distances (up to 90 mm) from the lung tumors. As illustrated in this figure, correlation coefficient behavior is unique for each tumor and depends on its site and type. For all tumors, correlation coefficient was almost the same and more than 95% up to 10 mm. The maximum correlation coefficient variation was observed for the right lung tumor behind rib#2 where this value reduced to less than 50% while the distance between tumor and clip reached 60 mm. In contrast, the correlation coefficient was almost superior for the left lung tumor up to 50 mm than for other tumors.

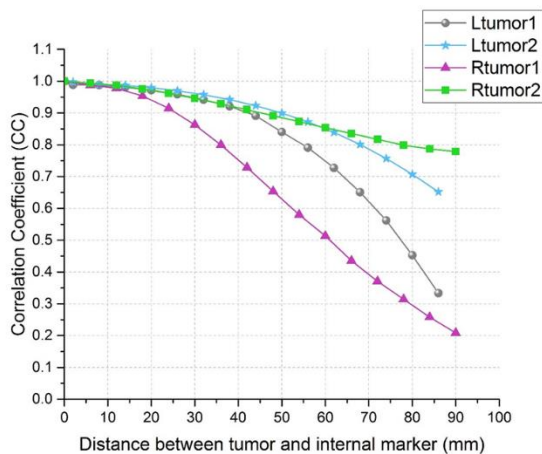


Figure 7. Correlation coefficient variation in the distances between tumor and clip

As illustrated in Figure 7, the correlation coefficient was reduced by increasing the distance between the tumor and the clip. Since the correlation coefficient was remarkably high while the clip was very close to tumor location, it is feasible to clinically implement this strategy.

Discussion

Successful radiotherapy involves the delivery of a 3D uniform dose to the target volume. This will be a challenging issue for the tumors that are located in the thorax region and move mainly due to respiration. In external surrogate radiotherapy, tumor position information must be tracked in real-time in order to keep dose uniformity. This requires the adoption of additional monitoring systems, in combination with external-internal markers, to estimate tumor motion during treatment using a consistent prediction model. In this technique, an internal clip is implanted inside or near tumor volume and represents tumor position during

treatment. However, the implanted clip may be problematic to keep dose uniformity, depending on its size, material, and location. Nonetheless, there are some concerns due to clip migration and its toxicity inside the patient body. Accordingly, in some cases, natural anatomical landmarks, such as the ribs of the diaphragm, are taken into account in place of clip utilization for tumor motion tracking.

The present study involved the assessment of the role of implanted clip in dose perturbation in conventional radiotherapy and hadron therapy. To this end, four beams, namely photon, electron, proton, and carbon ion, were taken into account as available therapeutic beams. In addition, dose perturbation caused by implanted clip was simulated inside a typical tumor volume, using Monte Carlo FLUKA code. All parameters of the simulation process, ranging from beam specifications to target parameters for each therapeutic beam, were assumed to be very close to those of a real treatment condition. Several internal markers that were different in size and material were considered during our simulation study, and a comparative study was performed among the four given therapeutic beams.

Moreover, a strategy was proposed to implant the clip outside the tumor volume to keep dose uniformity parameter. The most important challenge during the implementation of this strategy was whether the clip could still be a good representative of tumor motion or not. For this aim, an anthropomorphic XCAT phantom as a validated phantom was utilized to model the virtual situation of dynamic organs. This phantom facilitated the simulation of a typical internal clip at different distances from several lung tumors located behind the left and right ribs. The correlation between tumor motion and clip motion was investigated for four lung tumors located at different sites.

Based on the results presented in tables 3 and 4 and figures 5 and 6, the highest clip-induced dose perturbation was observed while the therapeutic beams were carbon ion and proton, respectively. It should be noted that dose variation in the upstream part was negligible, and the highest variation belonged to the downstream part of the clip. For all therapeutic beams, the amount of dose perturbation ranged from 4.42% (for photon) to 83.08% (for carbon ion using a large golden marker). The reason for the observed high dose variation for hadron beams is the physical concept of particle interaction with matters. For the proton and carbon ion, the amount of LET and energy deposition was remarkable in comparison to those for the rest of the available beams.

Based on our results, dose perturbation caused by implanted clips inside the tumor volume cannot be clinically ignored during hadron therapy. Regarding this, it is better to find a solution for this issue, such as using a smaller clip made of a material with a lower atomic number. To this end, in the current study, the clips were also simulated with three different sizes and the dose variations of each size were measured under the

same simulation condition. As seen in tables 3 and 4 and figures 5 and 6, dose perturbation was remarkably reduced while using a smaller clip for all therapeutic beams, compared to that observed for medium and large sizes. For instance, with regard to the carbon ion beam, this value was obtained as 4.14% and 83.08% for small and large clips, respectively. Therefore, a clip with a smaller size may yield a treatment with lower dose perturbation.

In the present study, a golden clip covered with PMMA with a low atomic number was also considered. As illustrated in the 6th columns of tables 3 and 4, the use of a combinational golden-PMMA clip resulted in a strong reduction in dose variation for all available beams. For carbon ion, dose variation was reduced up to 75.55%, compared to that observed for the golden clip of the same size. Therefore, the combinational clip led to a remarkable improvement. However, the concerning issue while using small and/or combinational clip was their sensitivity to mechanical resistance that must be considered during clip implantation.

Considering hadrons, dose perturbation at the upstream surface was much lower than that at the downstream one. However, this rate was higher for photon beams (Figure 6) because of the effect of back-scattered electron on dose distribution that was significant at the upstream part. With regard to other therapeutic beams, since the received dose was negligible due to back-scattered electron, compared to the high dose of therapeutic particles (i.e., electron, proton, and carbon ion), dose perturbation was not observed at the upstream part. As an example, for the large golden marker, this value was obtained as 2.58% and 8.69% for electron and photon beams, respectively.

Based on the results, in order to keep uniformity without perturbation, a strategy was proposed to implant the clip outside the tumor volume. To do this, four lung tumors located behind ribs 2 and 3 were taken into account by modeling a typical clip at different distances from tumors. These results are illustrated in Figure 7. The correlation coefficient was very high while the clip was very close to tumor position. In this regard, the correlation coefficient was estimated at > 98% when the clip was located at a distance of up to 11 mm from tumor location. Therefore, the implantation of the clip outside the tumor volume may be promising considering the reasonable correlation between tumor and clip motions.

The correlation coefficient for each tumor was variable while the slope of this parameter was high for the right lung tumor behind rib #2. It should be considered that the correlation coefficient is unique and must be calculated independently for each tumor located at different sites in the thorax region of the patient body. Future studies are recommended to investigate various combinational markers made of different materials. The proposed strategy can be tested in real condition assuming a natural anatomical landmark (instead of the implanted clip) that is located at a specific distance from a dynamic tumor so that the correlation coefficient

between tumor and natural landmark is measured. Moreover, it is suggested to consider correlation coefficients for further lung and liver tumors located at different sites and corresponding internal clips.

Conclusion

This study involved a comprehensive investigation of the effect of implanted clip on dose perturbation in conventional radiotherapy and hadron therapy. Since dose uniformity is one of the main objectives in hadron therapy, the role of implanted clip(s) on dose uniformity is crucial and must be taken into account. To this end, FLUKA code was utilized, and dose perturbation, with and without the presence of different markers of different dimensions and materials, was simulated against four therapeutic beams. The results showed that the effect of implanted clip on dose distribution was remarkable for proton and carbon ion therapy. Finally, in order to reduce dose perturbation, a strategy was proposed to find an optimum location for fiducial outside the tumor using the 4D XCAT anthropomorphic phantom. Final results confirmed the feasibility of implanting the clip outside tumor volume considering the correlation coefficient between tumor and clip motions.

Acknowledgment

The authors acknowledge Dr. Paul Segars for providing an anthropomorphic XCAT phantom.

References

1. Sorcini B, Tilikidis A. Clinical application of image-guided radiotherapy, IGRT (on the Varian OBI platform). *Cancer/Radiothérapie*. 2006 Sep 1;10(5):252-7.
2. Sorensen SP, Chow PE, Kriminski S, Medin PM, Solberg TD. Image-guided radiotherapy using a mobile kilovoltage x-ray device. *Medical Dosimetry*. 2006 Mar 1;31(1):40-50.
3. Huntzinger C, Munro P, Johnson S, Miettinen M, Zankowski C, Ahlstrom G, et al. Dynamic targeting image-guided radiotherapy. *Medical Dosimetry*. 2006 Jun 1;31(2):113-25.
4. Létourneau D, Martinez AA, Lockman D, Yan D, Vargas C, Ivaldi G, et al. Assessment of residual error for online cone-beam CT-guided treatment of prostate cancer patients. *International Journal of Radiation Oncology* Biology* Physics*. 2005 Jul 15;62(4):1239-46.
5. Mah D, Hanley J, Rosenzweig KE, Yorke E, Braban L, Ling CC, et al. Technical aspects of the deep inspiration breath-hold technique in the treatment of thoracic cancer. *International Journal of Radiation Oncology* Biology* Physics*. 2000 Nov 1;48(4):1175-85.
6. Rosenzweig KE, Hanley J, Mah D, Mageras G, Hunt M, Toner S, et al. The deep inspiration breath-hold technique in the treatment of inoperable non-small-cell lung cancer. *International Journal of Radiation Oncology* Biology* Physics*. 2000 Aug 1;48(1):81-7.

7. Berson AM, Emery R, Rodriguez L, Richards GM, Ng T, Sanghavi S, et al. Clinical experience using respiratory gated radiation therapy: comparison of free-breathing and breath-hold techniques. *International Journal of Radiation Oncology* Biology* Physics*. 2004 Oct 1;60(2):419-26.
8. Ford EC, Mageras GS, Yorke E, Rosenzweig KE, Wagman R, Ling CC. Evaluation of respiratory movement during gated radiotherapy using film and electronic portal imaging. *International Journal of Radiation Oncology* Biology* Physics*. 2002 Feb 1;52(2):522-31.
9. Ramsey CR, Cordrey IL, Oliver AL. A comparison of beam characteristics for gated and nongated clinical x-ray beams. *Medical physics*. 1999 Oct;26(10):2086-91.
10. Shirato H, Shimizu S, Kunieda T, Kitamura K, Van Herk M, Kagei K, et al. Physical aspects of a real-time tumor-tracking system for gated radiotherapy. *International Journal of Radiation Oncology* Biology* Physics*. 2000 Nov 1;48(4):1187-95.
11. Alnowam MR, Lewis E, Wells K, Guy M. Respiratory motion modelling and prediction using probability density estimation. In *IEEE Nuclear Science Symposium & Medical Imaging Conference 2010*;2465-2469.
12. Riaz N, Shanker P, Wiersma R, Gudmundsson O, Mao W, Widrow B, et al. Predicting respiratory tumor motion with multi-dimensional adaptive filters and support vector regression. *Physics in Medicine & Biology*. 2009 Sep 4;54(19):5735.
13. Ruan D. Kernel density estimation-based real-time prediction for respiratory motion. *Physics in Medicine & Biology*. 2010 Feb 4;55(5):1311.
14. Putra D, Haas OC, Mills JA, Burnham KJ. Prediction of tumour motion using interacting multiple model filter.
15. Ramrath L, Schlaefer A, Ernst F, Dieterich S, Schweikard A. Prediction of respiratory motion with a multi-frequency based Extended Kalman Filter. In *Proceedings of the 21st International Conference and Exhibition on Computer Assisted Radiology and Surgery (CARS' 07)*. 2007 ;21: 56-8.
16. Sahih A, Haas O, Burnham K, Mills J. Bilinear filter approach for internal and external respiratory motion modelling and prediction. In *Proc 16th Int' l Conf System Engineering*. 2006.
17. Goodband JH, Haas OC, Mills JA. A comparison of neural network approaches for on-line prediction in IGRT. *Medical physics*. 2008 Mar;35(3):1113-22.
18. Nguyen CC, Cleary K. Intelligent approach to robotic respiratory motion compensation for radiosurgery and other interventions. In *2006 World Automation Congress 2006* ;1-6.
19. Kakar M, Nyström H, Aarup LR, Nøttrup TJ, Olsen DR. Respiratory motion prediction by using the adaptive neuro fuzzy inference system (ANFIS). *Physics in Medicine & Biology*. 2005 Sep 21;50(19):4721.
20. Cedric XY, Jaffray DA, Wong JW. The effects of intra-fraction organ motion on the delivery of dynamic intensity modulation. *Physics in Medicine & Biology*. 1998 Jan;43(1):91.
21. Seppenwoolde Y, Shirato H, Kitamura K, Shimizu S, Van Herk M, Lebesque JV, et al. Precise and real-time measurement of 3D tumor motion in lung due to breathing and heartbeat, measured during radiotherapy. *International Journal of Radiation Oncology* Biology* Physics*. 2002 Jul 15;53(4):822-34.
22. Shirato H, Seppenwoolde Y, Kitamura K, Onimura R, Shimizu S. Intrafractional tumor motion: lung and liver. In *Seminars in radiation oncology 2004* ;14: 10-18.
23. Stevens CW, Munden RF, Forster KM, Kelly JF, Liao Z, Starkschall G, et al. Respiratory-driven lung tumor motion is independent of tumor size, tumor location, and pulmonary function. *International Journal of Radiation Oncology* Biology* Physics*. 2001 Sep 1;51(1):62-8.
24. Wu J, Lei P, Shekhar R, Li H, Suntharalingam M, D'Souza WD. Do tumors in the lung deform during normal respiration? An image registration investigation. *International Journal of Radiation Oncology* Biology* Physics*. 2009 Sep 1;75(1):268-75.
25. Liu HH, Balter P, Tutt T, Choi B, Zhang J, Wang C, et al. Assessing respiration-induced tumor motion and internal target volume using four-dimensional computed tomography for radiotherapy of lung cancer. *International Journal of Radiation Oncology* Biology* Physics*. 2007 Jun 1;68(2):531-40.
26. Torshabi AE, Pella A, Riboldi M, Baroni G. Targeting accuracy in real-time tumor tracking via external surrogates: a comparative study. *Technology in cancer research & treatment*. 2010 Dec;9(6):551-61.
27. Torshabi AE, Negarestani A, Pella A, Baroni G, Riboldi M, Rahnema M. A clinical application of fuzzy logic. *INTECH Open Access Publisher*; 2012 Mar 16.
28. Torshabi AE, Riboldi M, Fooladi AA, Mosalla SM, Baroni G. An adaptive fuzzy prediction model for real time tumor tracking in radiotherapy via external surrogates. *Journal of Applied Clinical Medical Physics*. 2013 Jan;14(1):102-14.
29. Balter JM, Sandler HM, Lam K, Bree RL, Lichter AS, Ten Haken RK. Measurement of prostate movement over the course of routine radiotherapy using implanted markers. *International Journal of Radiation Oncology* Biology* Physics*. 1995 Jan 1;31(1):113-8.
30. Crook JM, Raymond Y, Salhani D, Yang H, Esche B. Prostate motion during standard radiotherapy as assessed by fiducial markers. *Radiotherapy and oncology*. 1995 Oct 1;37(1):35-42.
31. Dehnad H, Nederveen AJ, van der Heide UA, van Moorselaar RJ, Hofman P, Lagendijk JJ. Clinical feasibility study for the use of implanted gold seeds in the prostate as reliable positioning markers during megavoltage irradiation. *Radiotherapy and oncology*. 2003 Jun 1;67(3):295-302.
32. van der Heide UA, Kotte AN, Dehnad H, Hofman P, Lagendijk JJ, van Vulpen M. Analysis of fiducial marker-based position verification in the external beam radiotherapy of patients with prostate cancer. *Radiotherapy and oncology*. 2007 Jan 1;82(1):38-45.
33. Riboldi M, Orecchia R, Baroni G. Real-time tumour tracking in particle therapy: technological developments and future perspectives. *The lancet oncology*. 2012 Sep 1;13(9):e383-91.
34. Chow JC, Grigorov GN. Dose measurements near a non-radioactive gold seed using radiographic film.

- Physics in Medicine & Biology. 2005 Aug 31;50(18):N227.
35. Newhauser W, Fontenot J, Koch N, Dong L, Lee A, Zheng Y, et al. Monte Carlo simulations of the dosimetric impact of radiopaque fiducial markers for proton radiotherapy of the prostate. *Physics in Medicine & Biology*. 2007 May 2;52(11):2937.
 36. Newhauser WD, Koch NC, Fontenot JD, Rosenthal SJ, Gombos DS, Fitzek MM, et al. Dosimetric impact of tantalum markers used in the treatment of uveal melanoma with proton beam therapy. *Physics in Medicine & Biology*. 2007 Jun 7;52(13):3979.
 37. Vassiliev ON, Kudchadker RJ, Kuban DA, Frank SJ, Choi S, Nguyen Q, et al. Dosimetric impact of fiducial markers in patients undergoing photon beam radiation therapy. *Physica Medica*. 2012 Jul 1;28(3):240-4.
 38. Giebeler A, Fontenot J, Balter P, Ciangaru G, Zhu R, Newhauser W. Dose perturbations from implanted helical gold markers in proton therapy of prostate cancer. *Journal of applied clinical medical physics*. 2009 Dec;10(1):63-70.
 39. Lim YK, Kwak J, Kim DW, Shin D, Yoon M, Park S, et al. Microscopic gold particle-based fiducial markers for proton therapy of prostate cancer. *International Journal of Radiation Oncology* Biology* Physics*. 2009 Aug 1;74(5):1609-16.
 40. Ptaszkiewicz M, Weber A, Swakon J, Klosowski M, Olko P, Bilski P, et al. Dose perturbation behind tantalum clips in ocular proton therapy. *Radiation measurements*. 2010 Mar 1;45(3-6):694-7.
 41. Herrmann R, Carl J, Jäkel O, Bassler N, Petersen JB. Investigation of the dosimetric impact of a Ni-Ti fiducial marker in carbon ion and proton beams. *Acta Oncologica*. 2010 Oct 1;49(7):1160-4.
 42. Cheung J, Kudchadker RJ, Zhu XR, Lee AK, Newhauser WD. Dose perturbations and image artifacts caused by carbon-coated ceramic and stainless steel fiducials used in proton therapy for prostate cancer. *Physics in Medicine & Biology*. 2010 Nov 12;55(23):7135.
 43. Zhang M, Kim S, Chen T, Mo X, Haffty BG, Yue NJ. Dose perturbations of gold fiducial markers in the prostate cancer intensity modulated proton radiation therapy (IMPT). 2012.
 44. Pontoriero A, Amato E, Iati G, De Renzis C, Pergolizzi S. Evaluation of the dose perturbation around gold and steel fiducial markers in a medical linac through Geant4 Monte Carlo simulation. *Journal of X-ray science and technology*. 2015 Jan 1;23(2):135-40.
 45. Segars WP, Sturgeon G, Mendonca S, Grimes J, Tsui BM. 4D XCAT phantom for multimodality imaging research. *Medical physics*. 2010 Sep;37(9):4902-15.
 46. Ferrari A, Ranft J, Sala PR, Fassò A. FLUKA: A multi-particle transport code (Program version 2005). Cern; 2005.
 47. Böhlen TT, Cerutti F, Chin MP, Fassò A, Ferrari A, Ortega PG, et al. The FLUKA code: developments and challenges for high energy and medical applications. *Nuclear data sheets*. 2014 Jun 1;120:211-4.
 48. Petoussi-Hens N, Bolch WE, Eckerman KF, Endo A, Hertel N, Hunt J, et al. ICRP Publication 116—the first ICRP/ICRU application of the male and female adult reference computational phantoms. *Physics in Medicine & Biology*. 2014 Aug 21;59(18):5209.
 49. Nankali S, Torshabi AE, Miandoab PS. A feasibility study on ribs as anatomical landmarks for motion tracking of lung and liver tumors at external beam radiotherapy. *Technology in cancer research & treatment*. 2017 Feb;16(1):99-111.
 50. Bond J, Frush J, Hon S, Eckersley C, Williams CH, Feng J, et al. Series of 4D adult XCAT phantoms for imaging research and dosimetry. In *Medical Imaging 2012: Physics of Medical Imaging* 2012;8313:83130P). International Society for Optics and Photonics.
 51. Segars WP, Bond J, Frush J, Hon S, Eckersley C, Williams CH, et al. Population of anatomically variable 4D XCAT adult phantoms for imaging research and optimization. *Medical physics*. 2013 Apr;40(4):043701.
 52. Geramifard P, Zafarghandi MS, Ghafarian P, Rahmim A, Ay MR. Respiratory-induced errors in tumor quantification and delineation in CT attenuation-corrected PET images: effects of tumor size, tumor location, and respiratory trace: a simulation study using the 4D XCAT phantom. *Molecular imaging and biology*. 2013 Dec;15(6):655-65.
 53. Samadi-Miyandoab P, Torshabi AE, Nankali S, Rezaei M. The robustness of various intelligent models in patient positioning at external beam radiotherapy. *Frontiers in Biomedical Technologies*. 2015 Mar 30;2(1):45-54.
 54. Samadi Miandoab P, Esmaili Torshabi A, Nankali S, Rezaei MR. A Simulation Study on Patient Setup Errors in External Beam Radiotherapy Using an Anthropomorphic 4D Phantom. *Iranian Journal of Medical Physics*. 2016 Dec 1;13(4):276-88.
 55. Nankali S, Torshabi AE, Miandoab PS, Baghizadeh A. Optimum location of external markers using feature selection algorithms for real-time tumor tracking in external-beam radiotherapy: a virtual phantom study. *Journal of applied clinical medical physics*. 2016 Jan;17(1):221-33.
 56. Miandoab PS, Torshabi AE, Nankali S. Investigation of the optimum location of external markers for patient setup accuracy enhancement at external beam radiotherapy. *Journal of applied clinical medical physics*. 2016 Nov;17(6):32-43.
 57. Samadi Miandoab P, Esmaili Torshabi A, Parandeh S. Calculation of inter- and intra-fraction motion errors at external radiotherapy using a markerless strategy based on image registration combined with correlation model. *Iranian Journal of Medical Physics*. 2019 May 1;16(3):224-31.
 58. Geramifard P, Zafarghandi MS, Ghafarian P, Rahmim A, Ay MR. Respiratory-induced errors in tumor quantification and delineation in CT attenuation-corrected PET images: effects of tumor size, tumor location, and respiratory trace: a simulation study using the 4D XCAT phantom. *Molecular imaging and biology*. 2013 Dec;15(6):655-65.
 59. Zaidi H, Tsui BM. Review of computational anthropomorphic anatomical and physiological models. *Proceedings of the IEEE*. 2009 Nov 17;97(12):1938-53.